Research Article

Journal of Environmental Nanotechnology

pH-tuned Mn-doped MoO_3 Nanoparticles for Photocatalytic Degradation of Sulfanilamide in Pharmaceutical Effluents

K. Kalaivani[1,2], N. Priyadharsini[3], S. S Boobesh[1], L. Jayanthi[1] and M. Elango[1*]

[1]Department of Physics, PSG College of Arts and Science, Coimbatore, TN, India
[2]Department of Physics, Sri Krishna College of Engineering and Technology, Coimbatore, TN, India
[3]Department of Physics, Dr. N.G.P. Institute of Technology, Coimbatore, TN, India
Received: 02.05.2025 Accepted: 22.06.2025 Published: 30.06.2025
*elango@psgcas.ac.in

ABSTRACT

Molybdenum trioxide (MoO_3) holds significant promise in fields such as photocatalysis, optoelectronics, and pharma effluent applications owing to its distinct structural, optical, and photocatalytic characteristics due to its tunable characteristics. Here, MoO_3 was synthesized with Manganese dopant through a simple wet-chemical method, with pH levels adjusted to 9.0, 10.0, and 11.0. Characterization techniques, including Structural analysis (XRD), field emission morphological analysis, photoluminescence, and optical spectroscopy, were employed to assess the material's properties. XRD results indicated minor changes in crystallite dimensions and lattice strain across different pH conditions, while FE-SEM images revealed morphological evolution from layered architectures to distributed nanoscale particles. PL and UV-Vis spectroscopy confirmed that the optical bandgap and defect-related emissions varied with pH, illustrating tunable optical behavior. Furthermore, the efficiency of degrading the Sulfanilamide was assessed using UV-Vis spectroscopy. To better understand the degradation mechanism, scavenger experiments were conducted, revealing that EDTA-2Na, a hole (h^+) scavenger, played a significant role, indicating that photogenerated holes are the primary active species in the process. Under UV light exposure, the Mn-doped MoO_3 nanocomposite demonstrated outstanding photocatalytic activity, achieving 84.7% degradation of Sulfanilamide – a removal of pharmaceutical effluent within 90 minutes.

Keywords: MoO_3/SiO_2; pH variation; Structural analysis; Morphological studies; Photocatalytic activity.

1. INTRODUCTION

Water pollution resulting from the discharge of pharmaceutical compounds by drug manufacturing industries has emerged as a significant environmental concern. These effluents are typically laden with both organic and inorganic contaminants due to the rapid expansion of industrial activities (Sathya *et al*. 2022). Even at trace levels, such pollutants can be highly toxic, posing serious health hazards to humans and aquatic organisms (Rathi *et al*. 2021). According to global estimates, approximately 3.2 million deaths occur annually due to the consumption of unsafe drinking water. Consequently, the removal of hazardous organic substances from water sources is of critical importance.

This study focuses on the sulfonamide group to act against gram-positive and gram-negative bacteria, protozoa. They are commonly prescribed for ailments such as urinary tract infections, ear and eye infections, vaginal and throat infections, and chronic bronchitis (Zhou *et al*. 2022). However, once discharged into aquatic environments, sulfonamides can persist and significantly disrupt ecosystems.

Researchers have a considerable interest in photodegrading these toxic pollutants into nontoxic or less toxic species for the environment. For this, several methods have been reported, such as adsorption, membrane process, ion exchange, and photocatalysis (P *et al*. 2025). Some of the above techniques cannot ultimate the drug residue, and it create secondary pollutants, which is again a challenge to remove. One promising approach to eliminating the pollutants is photocatalysis due to its ability to mineralize organic pollutants completely. Redox reactions on the drug surface are the fundamental basis of heterogeneous photocatalysis, and it is also a cost-effective, efficient method known for its ability to mineralize pollutants (Pattappan *et al*. 2023) entirely.

Semiconductor-based photocatalysts, particularly those derived from transition metal oxides, are highly suitable due to their diverse physicochemical properties. Ideal for this purpose. Among them, Molybdenum trioxide has received considerable attention owing to its excellent optical and electronic properties, multiple valence states, and high thermal and chemical stability. MoO3 can be identified in three different types of polymorphs: orthorhombic α-MoO3,

monoclinic β-MoO3, and hexagonal MoO3. In the meantime, MoO3's morphology and dimension have a substantial correlation with its performance. Multiple approaches are currently available for developing MoO3 nanoparticles with either a polycrystalline or amorphous microstructure (Sen *et al*. 2021). These NPs exhibit diverse morphologies, such as nanoribbons, hollow spheres, and flower-like structures (Nieto *et al*. 2024). Spherical MoO_3 NPs are particularly effective, offering high crystallinity, excellent colloidal stability, superior dispersibility, and large surface areas.

In this work, an Mn-doped MoO_3/SiO2 nanocomposite was successfully synthesized using the wet chemical method. The nanocomposite displayed large pores, a large surface area, and a low recombination rate, making it an ideal candidate for photocatalytic degradation. The photocatalytic of this nanocomposite was assessed by degrading Sulfanilamide pharmaceutical solution under visible light irradiation. Mechanistic studies revealed that photogenerated holes (h^+) play a critical part in the degradation process. Overall, the MoO3 with Manganese-doped nanocomposite proved to be an effective and ecologically responsive photocatalyst for removing pharmaceutical drug solutions.

2. PREPARATION PROTOCOL

All reagents used for the synthesis of Molybdenum trioxide (MoO_3) and its derivatives were of Analytical Reagent (AR) grade. Deionized (DI) water was used throughout all experimental procedures. The following chemicals were used without further purification: Hexaammonium heptamolybdate ($(NH_4)_6Mo_7O_{24}\cdot H_2O$), nitric acid ($HNO_3$), ammonia solution ($NH_4OH$), and manganese acetate ($Mn(CH_3COO)_2$), all procured from certified commercial suppliers.

2.1 Synthesis of 9 % Mn-doped MoO_3/SiO_2 Nanocomposites

A 0.2 M aqueous solution of Hexaammonium heptamolybdate was synthesized by dissolving the required amount in 100 mL of DI liquid under constant stirring for 30 minutes to ensure homogeneity. Subsequently, 25 mL of nitric acid was added dropwise under continuous stirring. Then, the solution was heated at 85 °C for 3 hours to facilitate precipitation. After 3 hours, the mixture was allowed to cool and reach room temperature. The final precipitate was white in color, washed and dried in a hot air oven at 130 °C for 12 hours, ground into a fine powder, and stored for further characterization.

For the preparation of 9% manganese-doped MoO_3 nanocomposites, a calculated quantity of manganese acetate was introduced into the precursor solution of Hexaammonium heptamolybdate during the initial mixing step. The pH of the solution was adjusted to 9, 10, and 11 during synthesis. The final product exhibited a light grey color, indicative of the formation of Mn-doped MoO_3. The precipitate was thoroughly washed, oven-dried at 130 °C, gently crushed into fine powder, and stored in an airtight container for further characterization.

2.2 Pharma Effluent Preparation

0.25 g of Sulfanilamide was mixed in 25 ml of water (1:1). Then, 1 ml of prepared solution was collected and mixed with 100 ml of water for stock solution. To achieve equilibrium, the dark stirring of the solution is required for 45 minutes. The UV light is illuminated for about 90 minutes, and 5ml of the mixer is collected at a systematic interval of every 30 minutes. After that, the samples were centrifuged at 3500 rpm speed for 5 min to eliminate the suspended particles. Fig. 1a represent the flowchart of processing of pharma effluent preparation. The photocatalytic degradation was monitored using a UV–visible spectrophotometer by measuring absorbance at a maximum wavelength of 258 nm.

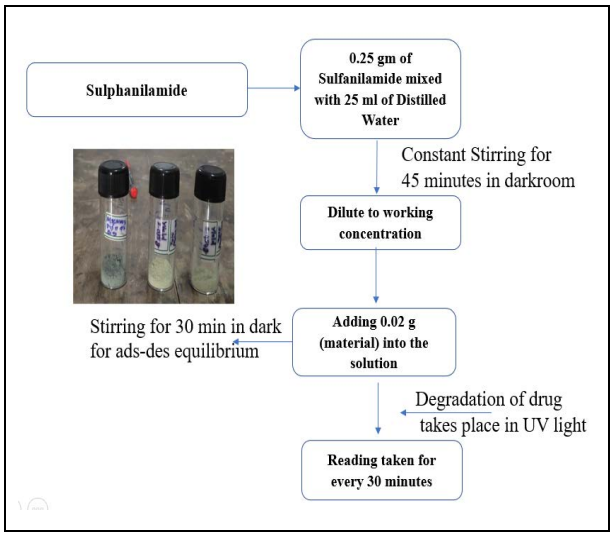


Fig. 1: (a) Flowchart for processing of Pharma effluent

3. RESULTS AND DISCUSSION

3.1 XRD Analysis

The X-ray diffraction (XRD) analysis of molybdenum trioxide (MoO_3) on SiO_2 matrix at pH 10.0 and Mn-doped MoO3 samples synthesized at pH levels 9.0, 10.0, and 11.0 provides valuable insights into their crystallinity and structural characteristics. All samples exhibit sharp and well-defined peaks corresponding to the orthorhombic phase of MoO_3, as confirmed by matching with the JCPDS No. 35-0569 reference data. The diffraction peaks observed in Fig. 1b show no significant phase transformation with pH variation, ensuring the phase purity of MoO_3 is maintained across all synthesis conditions (Kalaivani *et al*. 2025).

Quantitative analysis using the Scherrer equation reveals an average crystallite size, microstrain, and dislocation density of all samples, signifying the impact of pH on MoO_3 latices. Among the samples, the Mn-doped MoO_3 nanocomposite at pH 10 exhibits intense peaks and borders, indicating improved crystallinity. This improvement may be attributed to optimal nucleation conditions and better incorporation of Mn ions at this pH, which promotes the formation of well-defined crystal lattices. Table 1 gives the values of all samples.

Table 1. Lattice parameters of Mn doped MoO_3 nanoparticles

Sample	Crystallite Size (nm)	Microstrain	Dislocation Density x10^{-4}
MoO_3@SiO_2 pH 10.0	26.24	0.0997	1.45
Mn: MoO_3 pH 9.0	22.13	0.1098	2.04
Mn: MoO_3 pH 10.0	20.65	0.112	2.36
Mn: MoO_3 pH 11.0	24.31	0.1045	1.74

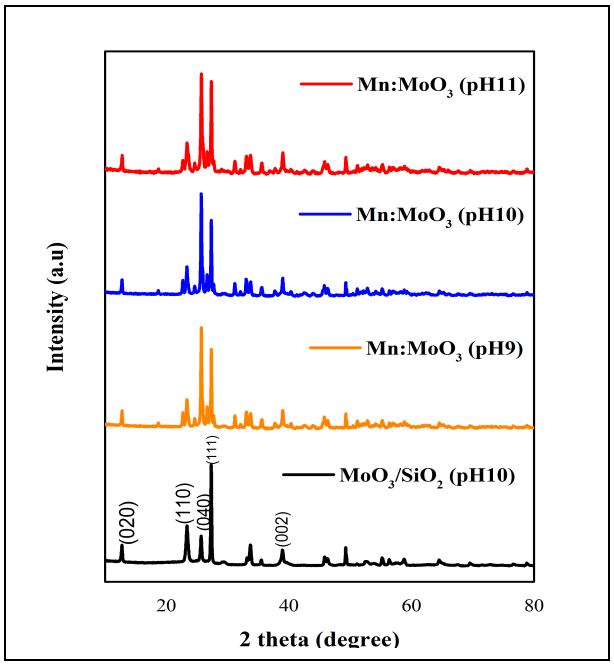


Fig. 1: (b) XRD diffractogram of Mn doped MoO_3 at pH 9.0, 10.0 and 11.0

Notably, the XRD patterns (Fig. 1b) demonstrate that samples synthesized at higher pH levels 10 exhibit sharper and more intense diffraction peaks compared to those at pH 9 and 11. This enhancement in peak sharpness and intensity indicates improved crystallinity and reduced structural defects under more alkaline conditions. The improved crystallinity at elevated pH can be credited to the increased availability of hydroxide ions, which promote uniform nucleation and growth dynamics, facilitating better coordination of MoO_6 octahedral. Conversely, at pH 11, the broader peaks and reduced intensity suggest higher defect densities and lattice distortions, likely due to incomplete deprotonation and less efficient nucleation processes.

The XRD analysis underscores the pivotal role of synthesis pH in modulating the structural integrity and crystallinity of MoO_3. Optimizing the pH during synthesis is crucial for tailoring the structural properties of MoO_3, which is essential for its advanced applications.

3.2 SEM Analysis

The scanning electron microscopy (SEM) analysis, presented in Fig. 2, reveals the critical influence of synthesis pH on the morphology of Mn-doped MoO_3 nanoparticles.

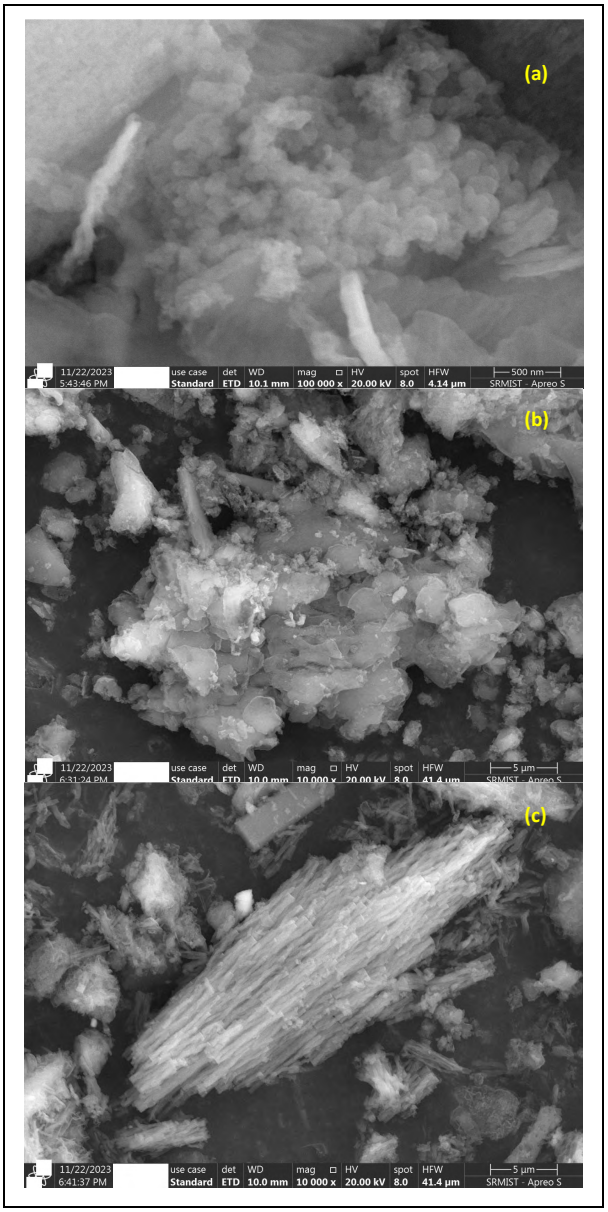


Fig. 2: SEM images of Mn doped MoO_3 at pH (a) 9.0, (b) 10.0 and (c) 11.0

At pH 9.0 (Fig. 2a), the particles exhibit a dense, layered micro particle with noticeable agglomeration, resulting reduced surface area. This is attributed to rapid nucleation and limited separation between grains under mildly acidic conditions. The average particle size at this pH, as estimated from SEM is approximately 26 nm. At pH 10.0 (Fig. 2b), a significant morphological transformation is observed. The particles appear smaller, more uniform, and less agglomerated, adopting a granular structure with improved porosity. This morphology reflects slower growth kinetics, which promotes better separation and prevents excessive aggregation (Nirmal *et al*. 2022). The particle size is reduced to about 21 nm, correlating with the lower crystallite size and enhanced dispersion. These parameters are advantageous for photocatalytic applications, where a high density of active sites is essential for improved performance. Conversely, at pH 11.0 (Fig. 2c), the particles begin to exhibit elongated, rod-like micro spindle shape features and show increased agglomeration compared to pH 10. The higher alkalinity promotes faster growth and anisotropic particle formation, leading to a slight increase in particle size (~24 nm) and partial clustering. This shift suggests a return to aggregation behavior, possibly due to over-saturation and the dominance of directional growth mechanisms at elevated pH levels (sen *et al*. 2024).

The results from XRD and SEM are in good agreement regarding the size evolution of Mn-doped MoO_3 nanoparticles. The crystallite sizes, calculated via the Scherrer equation, ranged from 20.65 nm to 24.31 nm, showing minimum crystallinity at pH 10.0. Similarly, SEM analysis reveals particle sizes in the range of 21–26 nm, supporting the observed trend of smaller, well-dispersed particles at pH 10.0 and increased agglomeration at pH 9.0 and 11.0. These observations confirm that the synthesis pH plays a pivotal role in tuning particle size, porosity, and morphology of the nanomaterials. Optimal features such as minimal agglomeration and uniform dispersion, essential for catalytic and optoelectronic applications, were achieved at pH 10.0.

3.3 PL Analysis

The photoluminescence (PL) spectra of Mn-doped MoO_3 nanoparticles synthesized at different pH levels are shown in Fig. 3. It provides critical insights into the optical emission behavior and defect state distributions influenced by synthesis conditions.

At pH 9.0 & 11.0, a prominent emission peak around 465 nm is observed, indicative of band-to-band recombination processes. The high intensity of these peaks suggests a well-crystallized structure with relatively fewer defect sites, resulting in efficient radiative recombination of electron-hole pairs. A noticeable decrease in PL intensity is observed at pH 10.0. This quenching of emission intensity indicates a reduction in radiative recombination of photogenerated electron–hole pairs, suggesting that the Mn-doped MoO_3 synthesized at pH 10.0 exhibits more efficient charge separation. The suppressed recombination is beneficial for enhancing photocatalytic activity, as it allows more charge carriers to participate in surface redox reactions during degradation of Sulfanilamide. This reduced intensity to the existence of shallow defect states due to interstitial vacancies, which introduce intermediate energy levels within the bandgap. These defects can trap the electrons and holes, resulting in radiative recombination at lower energy levels (Chakraborty *et al*. 2025). Additionally, the reduced PL intensity at this pH indicates an increase in non-radiative recombination centers, which can quench the overall emission.

The variations in PL behavior with pH focus on the critical role of synthesis protocol in modulating the defect landscape and electronic structure of MoO_3 nanoparticles. By fine-tuning the pH during synthesis, it is possible to control the optical properties of MoO_3, making it a promising candidate for applications in optoelectronics and photocatalysis.

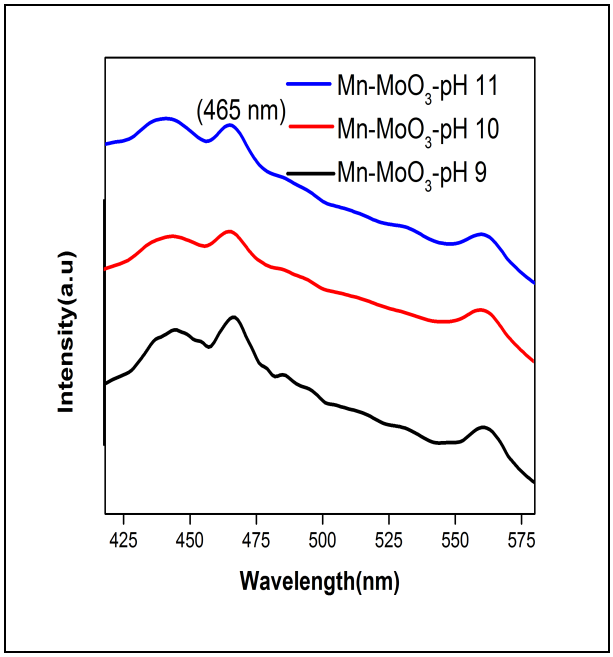


Fig. 3: Photoluminescence of Mn doped MoO_3 at pH 9.0, 10.0 and 11.0

3.4 UV Analysis

The UV-Vis absorption spectra of Mn-doped MoO_3 nanoparticles synthesized at varying pH levels demonstrate significant differences in their optical characteristics, highlighting the critical role of pH in tailoring material properties.

Optical Bandgap Determination: The band gap of Mn-doped MoO_3 samples at various pH can be determined by using the Tauc relation given as follow.

$$(\alpha h\nu)^2 = A(h\nu - E_g) \quad \ldots (1)$$

Where α is the absorption coefficient, h is the photon energy and is the band gap energy of the material. (Thiyagarajan *et al*. 2021)

Utilizing the Tauc plot method, the optical bandgap energies of the Mn-doped MoO_3 samples with various pH values of 9,10, and 11 were estimated to be 3.14, 3.09, and 3.06 eV, respectively. The doping of Mn with MoO_3 narrows its bandgap, and the bandgap energy values decrease by increasing the pH values. The intrinsic bandgap of orthorhombic MoO_3 affirms its semiconducting nature and potential for ultraviolet-driven photocatalytic applications.

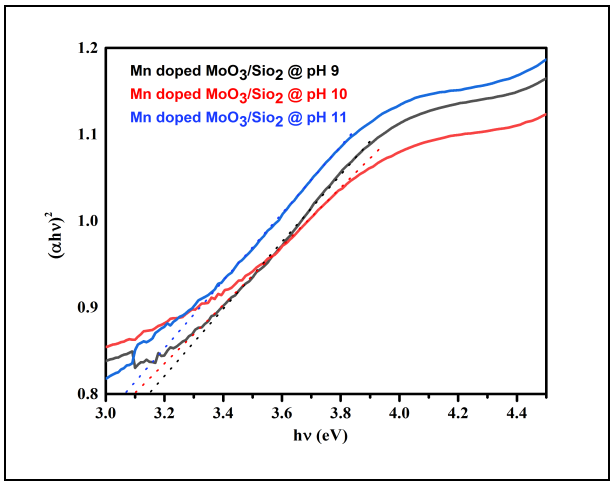


Fig. 4: Tauc plot of Mn doped MoO_3 at pH 9, 10 and 11

These findings of UV results emphasize the influence of synthesis pH on the optical properties of MoO_3 nanoparticles. Notably, the enhanced absorption observed at pH underscores its suitability for photocatalytic applications, where efficient light absorption and minimal defects are crucial for optimal performance.

3.5 TEM Analysis

TEM studies were carried out for synthesized Mn-doped MoO_3 nanocomposites at various pH levels 9.0,10.0 and 11.0. are illustrated in Fig. 5. The orthorhombic nanostructures resemble sphere-shaped and have interconnection among the particles. From the image, it is understood that the host and dopant merged to form a nano photocatalyst at 500 nm. It seems to have irregular morphology with agglomeration. In spite of these topography details, Mo-induced lattice distortions may influence and potentially enhance its catalytic performance.

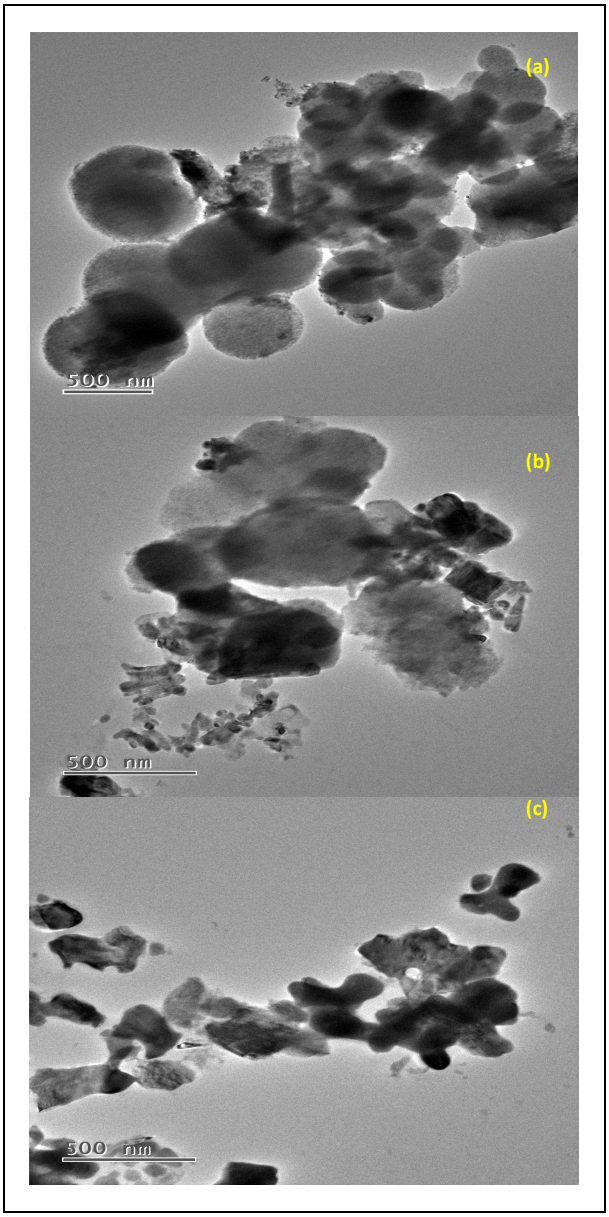


Fig. 5: TEM analysis of Mn doped MoO_3 prepared at pH (a) 9.0, (b) 10.0 and (c) 11.0

3.6 Photocatalytic Degradation of Mn-doped MoO_3 on Sulfanilamide

The photocatalytic degradation efficiency of Mn-doped MoO_3 nanoparticles synthesized at pH 10.0 was evaluated using Sulfanilamide drug under UV light irradiation. Fig. 6 shows the absorption spectra collected at different time intervals during the degradation process.

Initially, at 0 minutes, a prominent absorption peak is observed at 258 nm, accredited to the π–π* transitions in the aromatic ring of Sulfanilamide (Yan *et al*. 2025). This indicates a high concentration of the undegraded pharmaceutical compound. As UV irradiation proceeds, a noticeable reduction in peak intensity is seen at 30 minutes, suggesting the

photoactivation of Mn-doped MoO_3 and the initiation of oxidative degradation.

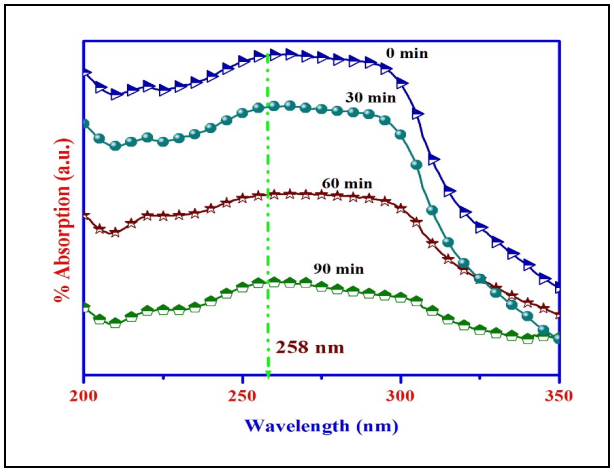


Fig. 6: UV–vis spectral degradation profile of Sulfanilamide under UV light using Mn-doped MoO_3 photocatalyst

The degradation continues progressively at 60 minutes, the peak diminishes further, and by 90 minutes, it nearly disappears, indicating substantial mineralization of Sulfanilamide into non-toxic byproducts such as CO_2, H_2O, and inorganic ions. Initially, the visual observation of the solution appeared faint yellow, attributed to the presence of Sulfanilamide drug. Upon exposure to UV light in the presence of the catalyst, a gradual fading of color was observed over time. After 90 minutes of irradiation, the solution became almost colorless, indicating effective photocatalytic degradation. This visual transformation strongly correlates with the UV–Vis spectral changes and confirms the breakdown of chromophoric groups in Sulfanilamide facilitated by Mn-doped MoO_3 nanoparticles.

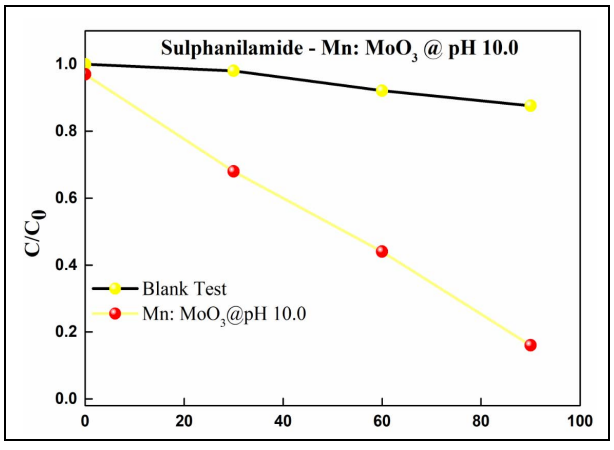


Fig. 7: (a) Degradation of Sulfanilamide under UV light with and without photocatalyst

To assess the contribution of photocatalysts, degradation studies were also performed without the catalyst. As shown in *Fig.* 7(a) & (b), the Sulfanilamide solution exposed only to UV light exhibited 12% degradation after 90 minutes. In contrast, the Mn-doped MoO_3 photocatalyst achieved 84.7% degradation efficiency under the same conditions, demonstrating excellent photoactivity.

To analyze the rate of reaction, a kinetic study was performed. The best-fit kinetics is first order equation as,

$$-In\left(\frac{C}{C_0}\right) = kt \qquad \ldots (2)$$

Where k is the rate constant, as illustrated in Fig. 8, the plot of $1/q_t$ vs. $1/t$ is linear with $R^2 = 0.9958$, indicating adherence to first-order kinetics, and the rate constant k was calculated to be 7.73×10^2 min^{-1}.

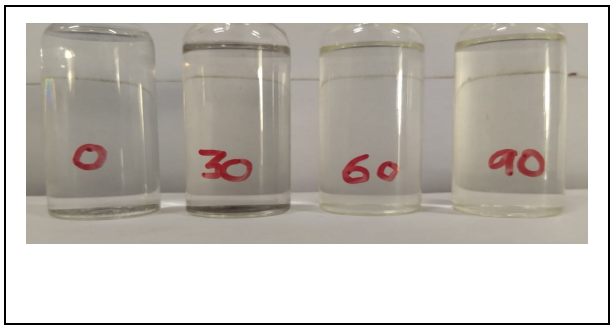


Fig. 7: (b) Degradation of Sulfanilamide under UV light for 90 min

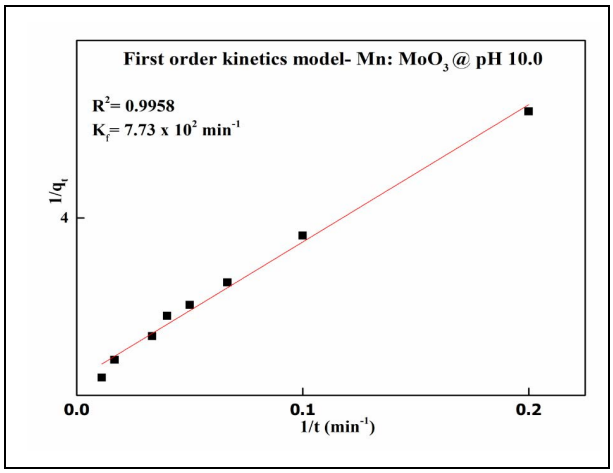


Fig. 8: First order kinetic plot for the photodegradation of sulfanilamide using Mn: MoO_3 (pH 10.0)

Fig. 8 represents the kinetic graph of Mn-doped MoO_3 exhibiting straight lines following the first-order reaction—the ability to harness light energy and promote the breakdown of persistent drug molecules into simpler compounds.

To explore the mechanism, reactive oxygen species (ROS) trapping experiments were conducted using scavengers: ethylenediaminetetraacetic acid

(EDTA) for holes (h^+), methanol for hydroxyl radicals, and benzoquinone for superoxide radicals. The degradation efficiency without any scavenger was 84.7%, which reduced to 78.6%, 56.7%, and 28.4% in the presence of h^+, •OH, and $O_2•^-$ scavengers, respectively (Fig. 9). These results confirm that holes play the dominant role in the photocatalytic process (Li *et al.* 2023), followed by hydroxyl and superoxide radicals.

Photogenerated electrons are excited from the valence band to the conduction band by UV irradiation, leaving the valence band with holes (h^+). These photogenerated carriers participate in redox reactions that degrade Sulfanilamide into environmentally benign products.

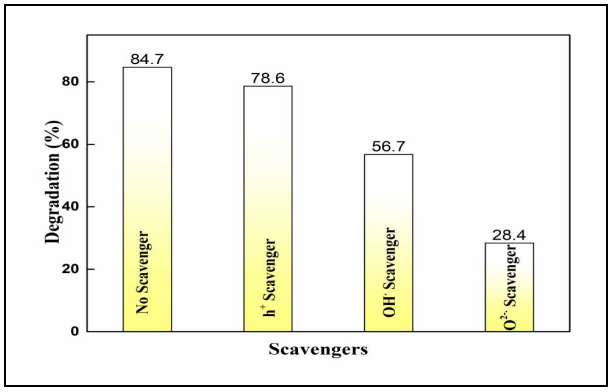


Fig. 9: ROS study of Mn: MoO_3 nanoparticles

3.6.1 Photocatalytic Degradation Mechanism

Upon UV irradiation, Mn-doped MoO_3 absorbs photons, exciting electrons from the valence band (VB) to the conduction band (CB), leaving behind holes (h^+). The Mn dopant introduces trap states that suppress charge recombination and enhance carrier separation.

Scavenger studies reveal that h^+ species are the dominant oxidative agents, directly oxidizing Sulfanilamide molecules and disrupting the aromatic, amide, and sulfonyl groups. A secondary contribution from •OH and $•O_2^-$ radicals support further degradation. The combined action results in cleavage of C–N and S–N bonds, leading to mineralization into CO_2, H_2O, and NH_4^+. The visual fading of the solution from colorless to pale yellow confirms the destruction of chemical structures.

4. CONCLUSION

In summary, we synthesized the Mn-doped MoO_3 at three different pH values, 9.0, 10.0, and 11.0, via a simple wet chemical method and utilized it as an effective photocatalyst for Sulfanilamide drug solution under UV light illumination. X-ray diffraction analysis, UV-Vis, and FESEM confirmed the nanoparticles. Photoluminescence (PL) analysis revealed that the Mn-doped MoO_3 synthesized at pH 10.0 exhibited the lowest recombination rate of charge carriers compared to those prepared at pH 9.0 and 11.0. The photocatalyst shows the degradation efficiency of 84.7% of the Sulfanilamide drug solution. Reactive species trapping experiments confirmed that photogenerated holes (h^+) played a dominant role in the degradation process. Furthermore, the reaction kinetics followed a pseudo-first-order model.

FUNDING

This research received no specific grant from any funding agency in the public, commercial, or not-for-profit sectors.

CONFLICTS OF INTEREST

The authors declare that there is no conflict of interest.

COPYRIGHT

This article is an open-access article distributed under the terms and conditions of the Creative Commons Attribution (CC BY) license (http://creativecommons.org/licenses/by/4.0/).

REFERENCES

Chakraborty, D., Priyadharsini, N. and Chaitanya, K., Color Center Defects on Modulating Magnetic, Optical, and Catalytic Behavior of Zinc Ferrites, *J. Mag. Mag. Mater.,* 628, 173183(2025). https://doi.org/10.1016/j.jmmm.2025.173183

Kalaivani, K., Boobesh, S. S., Janardhanan, P., Raffia, J. B., Priyadharshini, N. and Elango, M., Investigation of the Influence of pH on the Microstructure, Morphology, Optical Properties, and Environmental Remediation Efficacy of Molybdenum Trioxide (MoO_3), *Nanopart.*, 14(1), 582–89(2025). https://doi.org/10.13074/jent.2025.03.2511191

Li, Y., Yu, S., Xiang, J., Zhang, F., Jiang, A., Duan, Y., Tang, C., Cao, Y., Guo, H. and Ying, Z., Revealing the Importance of Hole Transfer: Boosting Photocatalytic Hydrogen Evolution by Delicate Modulation of Photogenerated Holes, *ACS Catal.*, 13(12), 8281–92(2023). https://doi.org/10.1021/acscatal.3c01210

Nieto, -P. E., Negrete, A. S., Ochando, M. I., Vondracek, M., Galiana, B., Pelaez, R. J., Mate, B., Lopez, A. S. and Serna, R., Building Nanoplatelet α-MoO_3 Films: A HighQuality Crystal Anisotropic 2D Material for Integration, *Appl. Surf. Sci.*, 672, 160871(2024). https://doi.org/10.1016/j.apsusc.2024.160871

Thiyagarajan, T., Venugopal, D., Raj, M., Joseph, C., Thangaraju, D., Baskaran, P., Hamdy, M. S. and Sh Facile synthesis and characterization of WO3/CuWO4 nanocomposites for the removal of toxic methylene blue dye, *Korean J. Chem. Eng.,* 38(5), 952–965(2021). https://doi.org/10.1007/s11814-021-0756-x

Nirmal, P. R. A., Biju, B. R., Joel, C., Hari, S. K. and Daniel, A. S., Systematic Analysis and the Effect of Mn Doping on Structural, Optical and Magnetic Properties of MoO_3 Nanoparticles, *Solid State Commun.,* 341, 114532(2022). https://doi.org/10.1016/j.ssc.2021.114532

Kavitha, P., Menaka, R., Jayaprakash, J., Nijarubini, V. and Priyadharshini, N., Visible Light-Driven Nd-ZnSe: Structural Insights and Enhanced Photocatalytic Degradation of Congo Red Dye, *Appl. Phy. A,* 131(6), 491(2025). https://doi.org/10.1007/s00339-025-08598-5

Pattappan, D., Amirthalingam, M., Rajendra, K. R. T., Sundararaj, P., Ting, Y. L., Yun, S. H., Jae, J. S. and Yuvaraj, H., Visible Light Photocatalytic Activity of a FeCo Metal-Organic Framework for Degradation of Acetaminophen and 2,4-Dichlorophenoxyacetic Acid and a Nematode-Based Ecological Assessment, *Chem. Eng. J.,* 464, 142676(2023). https://doi.org/10.1016/j.cej.2023.142676

Rathi, B. S., Senthil, K. P. and Dai, V. N., Critical Review on Hazardous Pollutants in Water Environment: Occurrence, Monitoring, Fate, Removal Technologies and Risk Assessment, S*ci. Tot. Environ.,* 797, 149134(2021). https://doi.org/10.1016/j.scitotenv.2021.149134

Sathya, K., Nagarajan, K., Malar, C. G. G., Rajalakshmi, S. and Raja, L. P., A Comprehensive Review on Comparison among Effluent Treatment Methods and Modern Methods of Treatment of Industrial Wastewater Effluent from Different Sources, *Appl. Water Sci.*, 12(4), 70(2022). https://doi.org/10.1007/s13201-022-01594-7

Sen, S. K., Suprita, D., Lincoln, P., Tapash, C. P., Manir, M. S., Mongur, H. and Hossain, M. N., Dy-Doped MoO_3 Nanobelts Synthesized via Hydrothermal Route: Influence of Dy Contents on the Structural, Morphological and Optical Properties, *J. Alloys Compd*., 876, 160070(2021). https://doi.org/10.1016/j.jallcom.2021.160070

Sen, S. K., Paul, M., Sakib, M. S. H., Manir, M. S., Hoque, K., Hawlader, R. S., Hasan, M. R. and Biswas, G. G., The effects of Mn doping on structural, morphological, and optical properties of hydrothermally synthesized h-MoO3 nanorods, *Ceram. Int.*, 50(7), 11565-11574 (2024). https://doi.org/10.1016/j.ceramint.2024.01.057

Yan, Z., Huiting, Y., Shuo, Z. and Zhiyong, T., Synergistic Interaction of Sulfonyl-Containing Sulfanilamide/Sulfamide to Enhance the Dielectric and Mechanical Properties of Polyurethane Materials, *Langmuir*, 41(19), 12324–36(2025). https://doi.org/10.1021/acs.langmuir.5c01203

Zhou, J., XIao, Y., Wang, J., Qi, L. and Yanli, W., A Review on the Ecotoxicological Effect of Sulphonamides on Aquatic Organisms, *Toxicol. Rep.*, 9, 534–40(2022). https://doi.org/10.1016/j.toxrep.2022.03.034